Aberrant splicing of U12-type introns is the hallmark of ZRSR2 mutant myelodysplastic syndrome

Vikas Madan[1], **Deepika Kanojia**[1,*], **Jia Li**[1,2,*], **Ryoko Okamoto**[3], **Aiko Sato-Otsubo**[4,5], **Alexander Kohlmann**[6,†], **Masashi Sanada**[4,5], **Vera Grossmann**[6], **Janani Sundaresan**[1], **Yuichi Shiraishi**[7], **Satoru Miyano**[7], **Felicitas Thol**[8], **Arnold Ganser**[8], **Henry Yang**[1], **Torsten Haferlach**[6], **Seishi Ogawa**[4,5], and **H. Phillip Koeffler**[1,3,9]

[1]Cancer Science Institute of Singapore, National University of Singapore, Singapore

[2]Department of Medicine, Yong Loo Lin School of Medicine, National University of Singapore, Singapore

[3]Cedars-Sinai Medical Center, Division of Hematology/Oncology, UCLA School of Medicine, Los Angeles, USA

[4]Cancer Genomics Project, Graduate School of Medicine, The University of Tokyo, Tokyo, Japan

[5]Department of Pathology and Tumor Biology, Graduate School of Medicine, Kyoto University, Kyoto, Japan

[6]MLL Munich Leukemia Laboratory, Munich, Germany

[7]Laboratory of DNA Information Analysis, Human Genome Center, Institute of Medical Science, The University of Tokyo, Tokyo, Japan

[8]Department of Hematology, Hemostasis, Oncology, and Stem Cell Transplantation, Hannover Medical School, Hannover, Germany

[9]National University Cancer Institute, National University Hospital Singapore, Singapore

Abstract

Correspondence and requests for materials should be addressed to V.M. (csivm@nus.edu.sg) or to H.Y. (csiyangh@nus.edu.sg).
†Present address: AstraZeneca, Personalized Healthcare and Biomarkers, Innovative Medicines, Cambridge, UK.
*These authors contributed equally to this work.

Somatic mutations in the spliceosome gene *ZRSR2* — located on the X chromosome — are associated with myelodysplastic syndrome (MDS). ZRSR2 is involved in the recognition of 3′ splice site during the early stages of spliceosome assembly; however, its precise role in RNA splicing has remained unclear. Here, we characterize ZRSR2 as an essential component of the minor spliceosome (U12-dependent) assembly. shRNA mediated knockdown of ZRSR2 leads to impaired splicing of the U12-type introns, and RNA-Sequencing of MDS bone marrow reveals that loss of ZRSR2 activity causes increased mis-splicing. These splicing defects involve retention of the U12-type introns while splicing of the U2-type introns remain mostly unaffected. ZRSR2 deficient cells also exhibit reduced proliferation potential and distinct alterations in myeloid and erythroid differentiation *in vitro*. These data identify a specific role for ZRSR2 in RNA splicing and highlight dysregulated splicing of U12-type introns as a characteristic feature of *ZRSR2* mutations in MDS.

Myelodysplastic syndromes (MDS) encompass a heterogeneous group of hematologic disorders collectively defined by aberrant differentiation of myeloid precursors in the bone marrow[1,2]. Because of the aging of our population, the incidence of the disease is increasing rapidly[3]. MDS is characterized by accumulation of abnormal myeloid precursors in the marrow which is accompanied by peripheral blood cytopenias. MDS often progresses to acute myeloid leukemia (AML), with a poorer prognosis compared to *de novo* AML[4,5]. Somatic mutations in several crucial genes including *TET2, DNMT3A, RUNX1, ASXL1, and EZH2* have been implicated as causal genetic alterations in MDS[6,7]. More recently, second generation sequencing of MDS identified a high frequency of somatic mutations in the genes encoding for the RNA splicing machinery[8]. Recurrent mutations were detected by us and others in *SF3B1, SRSF2, U2AF1, ZRSR2* and other spliceosome genes in independent cohorts of MDS, signifying a novel mechanism regulating the pathogenesis of this disease[9–14]. However, the functional consequence of these somatic mutations in the pathobiology of MDS remains largely unidentified.

RNA splicing is a fundamental process in eukaryotes which excises the intronic sequences from mRNA precursors to generate functional mRNA species. This function is carried out by the splicing machinery which comprises RNA-protein complexes called small nuclear ribonucleoprotein particles (snRNP). The major splicing machinery (termed U2 spliceosome) involves 5 snRNPs (U1, U2, U4, U5 and U6) which function in concert with numerous other proteins to effect splicing of introns[15]. In addition, a second class of introns processed by a divergent spliceosome called minor (or U12) spliceosome was later identified[16,17]. The U12 machinery consists of U11, U12, U4atac, U6atac and U5 snRNPs and recognizes distinct intronic splice sites[18–20]. The U12-type introns coexist with U2-type introns in several genes involved in essential cellular functions such as DNA replication, RNA processing, DNA repair and translation[21].

ZRSR2 (also known as *URP*) is located on X chromosome (Xp22.1) and encodes for a splice factor involved in recognition of 3' intron splice sites. It interacts with other components of the pre-spliceosome assembly including the U2AF2/U2AF1 heterodimer and SRSF2[22]. *In vitro* splicing assays suggest that ZRSR2 is required for efficient splicing of both the major and the minor class of introns[23]. In MDS, somatic mutations in *ZRSR2* occur across the

entire length of the transcript, which is in contrast to mutational hotspots observed in *SF3B1, SRSF2* and *U2AF1*. Moreover, nonsense, splice-site and frame-shift mutations in *ZRSR2* gene frequently occur in males, suggesting a loss of function. Mutations in *ZRSR2* are more prevalent in MDS subtypes without ring sideroblasts and chronic myelomonocytic leukemia (CMML), and are associated with elevated percentage of bone marrow blasts and higher rate of progression to AML[8,13]. However, the mechanism linking ZRSR2 deficiency to pathogenesis of MDS has not been explored.

In this study, we have evaluated the cellular and functional consequences of the loss of ZRSR2 in cell lines and patient samples. We show that ZRSR2 plays a pivotal role in splicing of the U12-type introns while the U2-dependent splicing is largely unaffected. MDS bone marrow harboring inactivating mutations in *ZRSR2* exhibit overt splicing defects, primarily involving the aberrant retention of U12-type introns. shRNA mediated knockdown of ZRSR2 similarly leads to impaired splicing of U12-type introns. Knockdown of ZRSR2 also inhibits cell growth and alters the *in vitro* differentiation potential of hematopoietic cells. This study uncovers a specific function of ZRSR2 in RNA splicing and also suggests its role in hematopoietic development.

RESULTS

Knockdown of ZRSR2 leads to specific splicing defects

In MDS, somatic mutations in *ZRSR2* are often inactivating alterations (nonsense, frame-shift and splice site mutations) which primarily affect the males, signifying its loss-of-function in these cases. To replicate the loss of ZRSR2, a lentiviral shRNA approach was used to stably downregulate its expression in human cells. Two shRNA vectors targeting ZRSR2 (ZRSR2 sh1 and sh2) were used to generate stable knockdown cells. These vectors resulted in efficient downregulation of *ZRSR2* transcript and protein levels in 293T cells and leukemia cell lines, TF-1 and K562 (Fig. 1a,b and Supplementary Fig. 1).

Firstly, we examined the effect of ZRSR2 deficiency upon splicing, by transfection of minigene constructs in ZRSR2 knockdown and control transduced 293T cells. Two reporter constructs commonly used to assess splicing – *P120* minigene[24] and *GH1* reporter plasmid[25] – were used in these experiments. *P120* minigene reporter consists of exons 5–8 of human *NOP2* (also known as *NOL1* or *P120*) gene. We observed that the splicing of intron F, a U12-type intron, was reduced upon downregulation of ZRSR2 using both ZRSR2 shRNA vectors (Fig. 1c,d). The *GH1* minigene reporter consists of three exons and upon transfection, a fully spliced and exon skipped (missing the second exon) mRNA can be detected. Notably, in a previous study, ectopic expression of mutant U2AF1 - a splice factor related to ZRSR2 and also frequently mutated in MDS - results in higher frequency of exon skipping from *GH1* minigene construct[12]. We observed that ZRSR2 knockdown and control 293T cells exhibited comparable rates of exon skipping upon transfection of *GH1* reporter construct (Supplementary Fig. 2). Therefore, our results highlight that ZRSR2 functions in a manner distinctive of U2AF1.

Next, we assessed splicing of endogenous introns in the MDS/AML cell line, TF-1[26], transduced with either ZRSR2 shRNA or control vector. ZRSR2 has been proposed to be

involved in splicing of both major and minor classes of introns[23], therefore, splicing of both these types of introns was examined. All tested U12-dependent introns were less efficiently spliced in the ZRSR2 knockdown cells (Fig. 1e,f). The average ratio of spliced/unspliced RNA for the ten U12-type introns was 0.30 in sh1 transduced and 0.38 in sh2 transduced cells as compared to 1.0 in the control cells. Notably, the splicing of six U2-type introns was not significantly affected (spliced/unspliced ratio of 1.19 for sh1 and 0.96 for sh2 as compared to 1.0 for cells transduced with control shRNA) (Fig. 1e,f). Hence, the inability of ZRSR2 knockdown cells to splice efficiently endogenous and exogenous U12-type introns points towards a specific defect in the minor splicing machinery.

To test if overexpression of ZRSR2 can rescue the U12 splicing defects, we transiently transfected wild-type ZRSR2 into stably knockdown 293T cells (Supplementary Fig. 3a) and measured the splicing efficiency of U12-type introns. Ectopic expression of ZRSR2 resulted in a significant increase in the splicing efficiency of all U12-type introns tested as compared to cells transfected with empty vector (Fig. 1g and Supplementary Fig. 3b). Therefore, we conclude that aberrant splicing observed in knockdown cells was a consequence of downregulation of ZRSR2. Overall, our experiments to evaluate splicing of endogenous and exogenous introns in ZRSR2 knockdown cells recognize its role in the U12 spliceosome.

Inactivating *ZRSR2* mutations in MDS cause splicing defects

To address the consequences of *ZRSR2* mutations in MDS, a global evaluation of splicing alterations was performed using RNA Sequencing (RNA-Seq). RNA was extracted from bone marrow of eight male MDS patients harboring either nonsense or frame-shift mutations of *ZRSR2* (Fig. 2a) (hereafter referred to as '*ZRSR2* mutant MDS'). We also sequenced RNA from four MDS cases without mutation in either *ZRSR2* or other commonly mutated splice factors (*U2AF1, SF3B1 and SRSF2*) (termed '*ZRSR2* WT MDS'). In addition, three non-malignant bone marrows and one remission bone marrow (remission of sample #7; *ZRSR2* mutant MDS) (Table 1) were also included as controls (termed 'normal BM'). RNA-Seq verified the presence of mutations in *ZRSR2* with a high mutant allele frequency (range 67.9%–98.0%) in all the *ZRSR2* mutant MDS samples (Supplementary Fig. 4).

First, the RNA-Seq data were examined for abnormal sequencing reads at all splice junctions to assess the extent of mis-spliced events in different groups. The 'normal' reads comprised of those which aligned to the known exon-exon junctions, while 'abnormal reads' spanned exon-intron junctions or corresponded to splicing involving an ambiguous splice site as illustrated in Fig. 2b. We examined 298,275 unique splice junctions (23,786 RefSeq transcripts in 15,737 genes) for aberrant splicing, and each *ZRSR2* mutant MDS sample was compared to a control sample (*ZRSR2* WT MDS or normal BM) as described in the Methods section. Using a false discovery rate (FDR) cutoff of 0.01 and difference in Mis-splicing Index (MSI)>20, significantly higher number of abnormally spliced junctions were detected in *ZRSR2* mutant MDS samples compared to the *ZRSR2* WT MDS samples in a majority of pairwise comparisons (Fig. 2c). Similarly, the number of such abnormal junctions was also elevated in *ZRSR2* mutant group when compared to four normal BM samples (Fig. 2d). These findings suggested a higher incidence of aberrant splicing in

samples with *ZRSR2* mutation as compared to controls. Notably, 689 mis-spliced junctions were identified in all eight *ZRSR2* mutant MDS cases, signifying a subset of introns which represent bona-fide downstream targets of ZRSR2.

ZRSR2 mutant MDS is characterized by aberrant intron retention

To delineate the splicing defects that occur in *ZRSR2* mutated cells, we carefully evaluated the RNA-Seq data of mutant and control bone marrows for aberrant intron retention, cryptic splice site usage and exon skipping. For identification of aberrant retention, introns with 95% coverage and with sequencing reads supporting both 5' and 3' exon-intron junctions were considered (described in Methods section). We compared the proportion of aberrant reads (spanning across both exon-intron junctions) in each sample to calculate the Mis-splicing Index (MSI) (Supplementary Fig. 5). The difference in the MSI values between the mutant and control samples (termed MSI) was used as a measure of aberrant retention for each intron. Using this approach, we tested 110,192 introns, and performed pairwise analyses between eight *ZRSR2* mutant MDS samples and eight controls (four *ZRSR2* WT MDS and four normal BM samples) to obtain 64 sets of comparisons. We observed that elevated number of retained introns was clearly evident in *ZRSR2* mutant MDS as compared to either *ZRSR2* WT MDS or normal BM samples (Fig. 3a,b). Importantly, significant intron retention was not detected when comparing the *ZRSR2* WT MDS to normal BM samples (Fig. 3c), underlining that the intron retention is specific to mutations in the *ZRSR2* gene.

We further examined the retained introns in *ZRSR2* mutated cases for the type of intron. The introns were categorized as either U2- or U12-type based on the divergence at the 5' and 3' splice sites and the branchpoint sequence[20,21], utilizing the computational method described previously[27]. This analysis revealed a striking overabundance of U12-type introns amongst the aberrantly retained introns in *ZRSR2* mutant MDS samples (Fig. 3a,b,d,e). This pattern was observed consistently across all the pairwise comparisons between *ZRSR2* mutant and control samples (Fig. 3d,e), while the comparisons between *ZRSR2* WT MDS and normal BM (16 pairwise comparisons) did not show any intron type-specific retention (Fig. 3f). Next, to ascertain the subset of introns which were consistently retained in *ZRSR2* mutant samples (MSI>20), we focused on introns recognized in a large number of pairwise comparisons. Expectedly, the number of retained introns identified in successively increasing numbers of pairwise comparisons gradually decreased (Supplementary Fig. 6), however, the proportion of U12-type introns among the retained introns steadily climbed (Fig. 3g). In fact, 43 out of 45 introns retained in the *ZRSR2* mutant MDS in all 64 comparisons were U12-dependent. On the other hand, specific intron retention in the *ZRSR2* WT and normal BM groups (MSI<-20) was not apparent, and no intron was retained in more than 41 pairwise comparisons (Fig. 3g). Consequently, amongst the high-ranking set of introns consistently retained (present in >41 pairwise comparisons) in the *ZRSR2* mutant MDS, a disproportionately higher prevalence (85%) of U12-type introns occurred (Fig. 3h and Supplementary Data 1), thereby, underscoring the involvement of ZRSR2 in the minor spliceosome machinery. Moreover, among the retained U2-type introns, 72% were contained in a transcript also harboring a U12-type intron, with the retained U2-type intron typically located immediately downstream of the U12-type intron (Fig. 3h and Supplementary Fig. 7). This indicates that the inefficient splicing of U12-type introns can

also cause mis-splicing of neighboring U2-type introns within the transcript. Only 11 U2-type introns which were independent of U12 transcripts were identified as aberrantly retained in our computational approach (Supplementary Data 1). These introns were indistinguishable from other unaffected U2-type introns (data not shown) and invariably displayed a weaker retention phenotype compared to the U12-type introns.

Though our preceding analysis identified that the U12-type introns were significantly retained in *ZRSR2* mutant MDS, we further inquired whether the splicing of all U12-type was affected. To address this, we examined the aberrant retention of each U12-type intron using the average MSI values for mutant vs control groups. Of all the genes harboring U12-type introns in the human genome[27, 28], genes containing 558 U12-introns were expressed at sufficient levels ($FKPM_{max}>1$; $FKPM_{average}>0.5$). Firstly, MSI calculations showed that practically all U12-type introns were mis-spliced, albeit to varying extent, in the *ZRSR2* mutant MDS group (Supplementary Fig. 8). This is also evident in individual pairwise comparisons between *ZRSR2* mutant MDS and control samples (Fig. 3d,e). Next, we classified the U12-type introns based on the MSI values and found that the splicing of only 29 introns (MSI 0) (5% of expressed U12-type introns) was unaffected (Supplementary Data 2). Although, we did not detect any difference in the distribution of GT-AG vs AT-AC intron type with the retention phenotype, the U12-type introns which are not retained in *ZRSR2* mutant cells tend to be longer (median length 1,958 nucleotides compared to 1,039 for significantly retained introns) (Supplementary Data 2). Interestingly, the unaffected GT-AG introns had relatively weaker splice sites as indicated by lower 5' splice site score compared to the retained introns (Supplementary Data 2).

We also sequenced mRNA from TF-1 cells in which ZRSR2 was downregulated using either sh1 or sh2 lentiviral vectors. Stable knockdown cells from two independent transduction experiments were used to examine for intron retention as described above. Expression analysis confirmed 60–70% reduction in *ZRSR2* transcript levels in the knockdown cells (Fig. 3i). The suppression of ZRSR2 in these knockdown cells resulted in marked retention of U12-type introns as compared to control shRNA transduced cells (Fig. 3j,k). Overall the number of retained introns obtained in knockdown TF-1 cells was lower than those identified in *ZRSR2* mutant MDS cases. This is conceivable because of low levels of ZRSR2 present in the knockdown cells as compared to complete absence in males with either nonsense or frame-shift mutations. Importantly, amongst the retained introns identified in both sh1 and sh2 knockdown cells, a large proportion were U12-type introns (Fig. 3l). Notably, we observed a sizable overlap of U12-type introns retained in both *ZRSR2* mutant MDS and knockdown TF1 cells (Supplementary Fig. 9).

Next, to validate the aberrant intron retention, quantitative RT-PCR (qRT-PCR) was used to measure the normalized intronic expression in *ZRSR2* mutant MDS and control samples. Using this approach, we tested eight representative U12-type introns detected as aberrantly retained in our computational analysis. We observed markedly higher expression of all tested introns in each of the mutant samples as compared to the control samples (Fig. 4a–h). In a parallel analysis, we also detected higher expression of these introns in ZRSR2 knockdown TF1 cells (Supplementary Fig. 10) signifying consistent findings in our two experimental models.

The experimental evidence of U12-type intron retention specifically in ZRSR2 deficient MDS samples further substantiates ZRSR2 as a crucial component of the U12-dependent spliceosome.

Additional mis-splicing events in *ZRSR2* mutant MDS

Further, using an approach similar to the one to detect intron retention, we searched for mis-splicing events involving abnormal recognition of 5' and 3' splice sites (Supplementary Fig. 5). We identified several loci where cryptic splice sites were observed in *ZRSR2* mutant MDS. We focused on loci which displayed aberrant splicing in all mutant cases and found that the majority of them were associated with transcripts containing U12-type introns. These events usually occurred either within the U12-type introns or in its vicinity. The incorrect recognition of splice sites resulted in a varied pattern of mis-splicing involving ambiguous splice donor and acceptor sites which invariably generated cryptic U2 splice junctions (Fig. 5). As representative examples of abnormal splice site recognition in *ZRSR2* mutant MDS, mis-spliced U12-type introns in *WDR41, FRA10AC1* and *SRPK2* genes were experimentally validated.

The intron 4 of human *WDR41* gene is a U12-type intron. RNA-Seq revealed a distinctive pattern of mis-splicing in all *ZRSR2* mutant samples which includes retention of the 5' portion of intron followed by multiple mis-splicing events employing cryptic U2-type splice sites within the intron 4 (Fig. 5a,b and Supplementary Data 3,4). We verified presence of such aberrant splice junctions across exons 4 and 5 involving the two cryptic exons (4A and 4B) using qRT-PCR. The levels of mis-spliced products were substantially higher in the *ZRSR2* mutant MDS as compared to either the *ZRSR2* WT MDS or normal BM samples (Fig. 5c,e). Moreover, Sanger sequencing of the products amplified from *ZRSR2* mutant samples verified the predicted splice junctions (Fig. 5d,f). We detected two alternative splice donor sites (4' and 4" located 19 bp apart) both of which resulted in splicing to cryptic exon 4A (Fig. 5g,h). Similarly, in *FRA10AC1* and *SRPK2*, anomalous splice junctions were created from cryptic U2-type splice sites which resulted in partial retention of U12-type introns in *ZRSR2* mutant samples (Fig. 5i,j, Supplementary Fig. 11a,b and Supplementary Data 3,4). The presence of these alternative splicing junctions was also validated by PCR and Sanger sequencing (Fig. 5k,l and Supplementary Fig. 11c,d). Likewise, in conventional RT-PCR analysis of *WDR41, FRA10AC1* and *SRPK2*, aberrantly spliced transcripts were detectible only in ZRSR2 mutant MDS samples (Supplementary Fig. 12).

We also detected a few instances of increased exon skipping in the *ZRSR2* mutant group. The exon skipping was observed in the transcripts containing the U12-type introns and often involved exons flanking the U12-type intron (Supplementary Data 5).

Downregulation of ZRSR2 alters growth and differentiation

We investigated the consequences of ZRSR2 suppression upon cell growth and hematopoietic differentiation using shRNA mediated knockdown. We observed that the ZRSR2 deficient leukemia cells divided moderately slower than the cells transduced with control shRNA vector (data not shown). In soft agar colony assay, downregulation of ZRSR2 resulted in pronounced reduction in the number of colonies obtained in TF-1 and

K562 cells (Fig. 6a). In Propidium Iodide staining of steady state TF-1 cells, fewer cells were detected in S-phase of the cell cycle (Supplementary Fig. 13a). Also, lower proportion of ZRSR2 knockdown cells incorporated BrdU in *in vitro* labeling assay (Supplementary Fig. 13b), indicating that ZRSR2 deficient cells divide slower than the control cells. We further tested the *in vivo* tumorigenic potential of ZRSR2 knockdown K562 cells in mice. Cells were injected subcutaneously in NSG mice, and the tumor growth was assessed. ZRSR2 deficient K562 cells produced smaller tumors as compared to the cells transduced with control shRNA (Fig. 6b). These results illustrate that downregulation of ZRSR2 suppresses cellular growth both *in vitro* and *in vivo*.

Next, the implications of ZRSR2 deficiency on myeloid differentiation were investigated using an *in vitro* model of differentiation of human CD34+ hematopoietic stem cells (HSCs). CD34+ cells enriched from cord blood were transduced with either ZRSR2 shRNA or control shRNA lentivirus and analyzed for *in vitro* clonogenic growth in methylcellulose media. We observed a marked decrease in the number of BFU-E colonies obtained after 9 days. On the other hand, a notable increase in CFU-M colonies occurred while the number of CFU-G colonies was unaffected (Fig. 6c). We confirmed an effective knockdown of *ZRSR2* in transduced cells using qRT-PCR (Supplementary Fig. 14). Next, we evaluated the differentiation profile of CD34+ cells using flow cytometry. Following transduction with lentivirus, cells were cultured in the presence of cytokines for 2 weeks. A significant increase in the proportion of CD11b+ myeloid cells was observed in cultures upon knockdown of ZRSR2 (Fig. 6d,e). Downregulation of ZRSR2 also resulted in a reduced proportion of erythroid precursors co-expressing Glycophorin A and CD71 surface antigens (Fig. 6f,g). These results indicate that suppression of ZRSR2 alters erythroid and myeloid differentiation of HSCs, presumably as a result of dysregulated splicing of genes implicated in hematopoiesis.

Pathways regulated by mis-spliced genes in *ZRSR2* mutant MDS

To reveal the enrichment of functionally related genes among the significantly mis-spliced transcripts in *ZRSR2* mutant MDS (Supplementary Data 1,4,5), Gene Ontology (GO) analyses was performed using the standard enrichment computation method. A significant enrichment was obtained for several pathways (p<0.05) including mitogen-activated protein kinase (MAPK) signaling, ErbB signaling and for genes associated with chronic myeloid leukemia and acute myeloid leukemia (Fig. 7a). We sought to identify downstream targets of aberrant splicing of ZRSR2 which may contribute to the disease phenotypes. Several genes which participate in either hematopoietic differentiation or are implicated in myeloid malignancies were consistently mis-spliced in all *ZRSR2* mutant MDS samples (Fig. 7b). For instance, members of E2F transcription factors - E2F1, E2F2, E2F3, E2F4 and E2F6 - which function during myeloid differentiation[29–35] exhibit splicing defects in *ZRSR2* mutant cells. Similarly, various regulators of MAP kinase signaling, including MAPK1, MAPK3, RAS guanyl releasing proteins and RAF serine/threonine protein kinases contain U12-type introns and were mis-spliced in *ZRSR2* mutant cells. These proteins mediate vital signaling cascades and their role in maintaining physiological hematopoiesis has been identified[36–44]. Another interesting candidate is the tumor suppressor gene, *PTEN*, loss of which impairs HSC activity, alters their lineage commitment and leads to myeloid disorders in mice[45,46].

Dysregulation of these genes through aberrant splicing can potentially have direct implications upon hematopoietic differentiation and may contribute to the pathogenesis of MDS. Further investigations are necessary to identify effector(s) of the MDS phenotype in *ZRSR2* mutant cells.

Overall, our results demonstrate that *ZRSR2* mutations lead to aberrant splicing, primarily involving U12-type introns. These splicing defects are also corroborated in knockdown cells which display alterations in growth and differentiation, substantiating an essential and non-redundant role of ZRSR2 in the U12-dependent spliceosome.

DISCUSSION

Discovery of mutations in several spliceosome genes in MDS strongly suggest existence of dysfunctional splicing machinery in this disease. Interestingly, majority of the mutated genes including *SF3B1, U2AF1, ZRSR2, SRSF2, SF1* and *SF3A1*[8], encode for components of E/A splicing complex which is involved in the recognition of splice sites. Recurrent somatic mutations in these genes which occur mutually exclusively indicate that the disruption of initial splicing steps is a common feature in MDS. Therefore, these mutations can be predicted to cause widespread alterations in splicing and gene expression. However, contrary to this hypothesis, mutations in *U2AF1* and *SF3B1* exert splicing changes in a specific subset of introns and exons[11,47,48]. Hence, this raises the question whether each splice factor mutations has a distinctive effect on the splicing machinery which possibly results in diverse phenotypes. In fact, evidence shows an association between splice factor mutation and the clinical phenotype. *SF3B1* mutations are found at high frequency in MDS subtypes characterized by presence of ring sideroblasts, *SRSF2* mutations are highly associated with CMML, while mutations in *ZRSR2* are often observed in RAEB-1 and RAEB-2 subtypes[8,13,47,49–52] In this study, we demonstrate that the depletion of ZRSR2 leads to a specific splicing defect by disrupting the splicing of the entire subset of U12-type introns. Therefore, our study and previous reports indicate that the mutations in individual splice factors are likely to alter the function of splicing machinery in an exclusive manner.

Our results define an essential role of ZRSR2 in splicing of U12-type introns and propose it as one of the key components of the minor spliceosome. Our lentiviral shRNA mediated knockdown approach demonstrates a specific defect in splicing of U12-type introns which can be reversed by transient overexpression of ZRSR2. Most notably, RNA-Seq revealed that the transcriptome of *ZRSR2* mutant MDS exhibited several splicing defects, invariably resulting from inefficient splicing of U12-type introns. Surprisingly, the U2-type introns were spliced with similar efficiency as the control cells. Although ZRSR2 has been shown to be also required for *in vitro* splicing of U2-type introns[22,23], our results provide the first evidence that *in vivo* splicing of U2-type introns is essentially unaffected in the absence of ZRSR2. We detect significant retention of U2-type introns only in transcripts which contain U12-type introns. Rare U2-type introns independent of U12 transcripts appear in our analysis of mis-spliced introns. However, these introns exhibit weak mis-splicing phenotype and do not indicate any specificity with respect to either splice site strength or intron length, and therefore, are likely outliers in our analysis. These results signify ZRSR2 is crucial to U12 spliceosome machinery while it may have either a limited or redundant role in the U2

machinery. Additionally, ZRSR2 has been identified as a component of U11/U12 snRNP[53] and also a crucial role of ZRSR2 in U12-dependent spliceosome was also noted by the inability of cell extract lacking ZRSR2 to form a U12 splicing complex assembly in *in vitro* assays[23]. Further, a perfect correlation exists in the phylogenetic distribution of organisms that have both ZRSR2 and U12-dependent splicing, which also strongly supports the involvement of this splice factor in the U12 machinery[23]. Our computational analysis also demonstrates that *ZRSR2* mutations cause mis-splicing of a majority of U12-type introns, except for a minor subset with weaker U12-type splice sites.

ZRSR2 contacts the 3' splice site of the U12-type intron of *P120* transcript by binding the A residue of the AC dinucleotide at the 3' splice site[23]. This suggests that ZRSR2 is needed for recognition of 3' splice sites in U12-type introns. Interestingly, the U12-spliceosome complexes (Complex A and Complex B/C) failed to assemble at *P120* pre-mRNA in its absence[23], indicating that recognition of the whole intron is impaired. Analysis of our RNA-Seq data also suggests that the ZRSR2 mediated 3' splice site recognition is required for the 5' splice site and branch site recognition. This is evident by activation of cryptic 5' splice site sequences in certain U12-type intron containing transcripts like DRAM2, TAPT1, VPRBP etc. in *ZRSR2* mutant MDS (Supplementary Fig. 15). Similar instances of cryptic splice sites were previously reported for deficiency of RNPC3 and U11–48K, proteins also involved in the U12 splicing machinery[54,55]. The cryptic splice junctions observed in *ZRSR2* mutant cells were invariably U2-type.

Unlike the U2-dependent spliceosome, the U12-dependent machinery has been less well understood and proteins involved in splice site recognition are not clearly defined. U12 spliceosome was initially uncovered as a machinery instrumental in excising introns lacking the consensus GT-AG splice site termini[56]. However, it was soon recognized that this splicing complex was responsible for a unique subset of evolutionary conserved introns which had a highly conserved splice site recognition sequences distinct from the U2-type introns[16,17,21,24] and which utilized different snRNPs than those used in U2 machinery[18,19]. Although the U12-type introns comprise ~ 0.5% of all human introns, they exist in several crucial genes involved in vital cellular processes[57]. Germline mutations in the *RNU4ATAC* gene, which encodes for an essential component of the U12 spliceosome, have been shown to cause MOPD1/TALS (Microcephalic Osteodysplastic Primordial Dwarfism type 1 / Taybi-Linder Syndrome), a rare developmental disorder in humans[58,59]. Biallelic mutations in *RNPC3* gene which encodes for a 65 kDa constituent of U11/U12 di-snRNP also lead to isolated familial growth hormone deficiency[55]. Moreover, an intact U12 spliceosome is essential for the development of Drosophila (despite the presence of <20 U12-type introns in its genome) and zebra fish[60–62]. Thus, the questions raised in the context of myeloid neoplasms are: what are the consequences of the impairment of U12 splicing specifically in hematopoietic stem cells and how the *ZRSR2* mutations (and other spliceosome gene mutations, in general) contribute to leukemogenesis. We show that knockdown of ZRSR2 in human HSCs alters their *in vitro* differentiation potential. Reduced differentiation occurs towards erythroid lineage accompanied by a higher proportion of CD11b+ myeloid cells upon knockdown of ZRSR2. These results suggest that a competent U12 spliceosome is required for normal myeloid differentiation. Further investigations will focus on identifying

downstream target genes, which upon mis-splicing lead to pathogenic consequences in MDS. In this study, the GO analysis of U12-type genes identifies few such molecular pathways with potential involvement in the MDS phenotype. We find that genes encoding E2F transcription factors and several components of the Ras/Raf/MEK/ERK signaling exhibit aberrant splicing of U12-type introns consistently in all *ZRSR2* mutant MDS. These proteins have been implicated in normal and malignant hematopoiesis and represent possible candidates for future investigations. Studies using murine models will help identify downstream targets and better understand the role of ZRSR2 mediated splicing in hematopoietic differentiation. Pathway analysis of mis-spliced genes also revealed a strong enrichment of key cellular functions such as RNA transport, cell cycle, cellular response to stress, response to DNA damage stimulus, protein transport, protein serine/threonine kinase activity and ribonucleotide binding among the mis-spliced genes (Supplementary Fig.16). These functional classes have been previously attributed to the genes containing the U12-type introns[57].

Downregulation of ZRSR2 impaired *in vitro* clonogenic ability and suppressed tumor formation in mice. Overall, the ZRSR2 knockdown leukemia cells showed a general tendency to grow slower than the control cells. This observation is similar to the effect on cell growth reported for other spliceosome mutations. Expression of mutant *U2AF1* suppressed the growth of cell lines and resulted in lower reconstitution potential in mice[8]. Cell cycle arrest and inhibition of growth in leukemia cell lines is also attributed to downregulation of SF3B1[63]. Therefore, the spliceosome mutations do not seem to contribute towards a proliferative advantage of the hematopoietic precursors in MDS. How these cells harboring spliceosome mutations achieve clonal expansion remains unclear. One explanation can be that other accompanying genetic alterations are necessary to confer a proliferative advantage. In fact, mutations in several components of epigenetic machinery co-occur with spliceosome mutations. A high incidence of co-occurrence of mutations in the *TET2* and *ZRSR2* genes has been noted in MDS[8,13]. Loss of TET2 has been shown to lead to myeloproliferation and transformation of hematopoietic precursors in mice[64,65]. Therefore, mutations in *TET2* are likely to promote clonal dominance. Mutations in spliceosome genes, which occur early during leukemogenesis[66], might play a prominent role in modifying the differentiation potential of myeloid precursors, thus contributing to abnormal precursor phenotype, which is a hallmark of MDS. Further studies into co-operativity between mutations in spliceosome and epigenetic modifier genes in pathogenesis of myeloid disorders are therefore warranted.

METHODS

Generation of stable ZRSR2 knockdown cell lines

Lentiviral shRNA vectors (pLKO.1) were either purchased from Sigma or assembled by cloning the shRNA hairpin loop sequence into the AgeI/EcoRI sites of the empty vector. The target sequence for the ZRSR2 shRNAs sh1 and sh2 are 5'-CAACAGTTCCTAGACTTCTAT-3' and 5'-AGCAGCCCTTTCTCTGTTTAA-3', respectively. MISSION pLKO.1-puro Non-Mammalian shRNA Control (SHC002; Sigma) was used as control vector for transduction. To generate lentiviral particles, 293T cells

(kindly provided by Dr. Bing Lim, Genome Institute of Singapore, Singapore) were co-transfected with shRNA plasmid and the packaging plasmids, pMISSIONgagpol and pMISSIONvsvg (Sigma) using Lipofectamine 2000 (Invitrogen). Virus containing supernatant was collected after 48 and 72 hours, filtered through 0.45 μm filter and stored in aliquots at −80°C. TF-1 and K562 cells (American Type Culture Collection) were infected with lentivirus for 2 rounds, 24 hours apart, in the presence of 5 μg/ml protamine sulfate. Transduced cells were selected in puromycin to generate stable knockdown cell lines. The knockdown was verified using qPCR and western blotting.

Western blot analysis

Total protein lysates were prepared using M-PER Mammalian Protein Extraction Reagent (Thermo Scientific) containing protease inhibitor cocktail (Roche). 25 μg protein was resolved on 10% SDS-PAGE gel and transferred to Immobilon-P PVDF membrane (Millipore). Anti-ZRSR2 antibody (1:2500 dilution) (kindly provided by Dr Michael Green, University of Massachusetts Medical School, Massachusetts) was used to determine ZRSR2 protein expression. The membrane was stripped before probing with anti-GAPDH antibody (1:5000 dilution) (Cell Signaling Technology).

Minigene splicing assays

P120 reporter construct was generously provided by Dr Richard A. Padgett, Cleveland Clinic, Cleveland, Ohio and the *GH1* minigene plasmid was provided by Dr Kinji Ohno, Center for Neurological Diseases and Cancer, Nagoya, Japan. 293T cells were transfected with *P120* or *GH1* plasmids using jetPRIME transfection reagent (Polyplus Transfection SA). Briefly, cells in 60mm dish were transfected with 200 ng of reporter plasmid. Cells were harvested 48h after transfection, and total RNA was extracted using AxyPrep Multisource Total RNA Miniprep Kit (Axygen). RNA was treated with DNase I followed by cDNA synthesis using RevertAid First Strand cDNA Synthesis Kit (Thermo Scientific). For *P120* minigene assay, plasmid specific primer was used for reverse transcription. The cDNA was used as a template to amplify the region of *P120* gene containing intron F at 94°C for 2 min followed by 25 cycles of 94°C for 30 sec, 60°C for 40 sec, 72°C for 40 sec and a final extension at 72°C for 7 min. Amplified PCR product was resolved on agarose gel, stained with ethidium bromide and photographed. Bands corresponding to spliced (112 bp) and unspliced (211 bp) products were quantified using Image Lab software (Biorad).

For *GH1* minigene, reverse transcription was performed using random primers. The PCR to amplify the *GH1* transcript was performed at 94°C for 2 min followed by 28 cycles of 94°C for 30 sec, 60°C for 40 sec, 72°C for 40 sec and a final extension at 72°C for 7 min. Amplicons corresponding to fully spliced and exon skipped transcripts measured 447 bp and 327 bp, respectively. The sequences of primers used for RT-PCR are provided in the Supplementary Table 1.

RT-PCR to determine splicing efficiency of U2-type and U12-type introns

Splicing of U2-type and U12-type introns was measured using qRT-PCR[47,59]. Briefly, RNA was treated with DNase I (Thermo Scientific) followed by reverse transcription using RevertAid M-MuLV Reverse Transcriptase (RevertAid First Strand cDNA Synthesis Kit;

Thermo Scientific) in the presence of random primers. Spliced and unspliced levels of introns were measured using two separate qPCRs and normalized to *GAPDH* transcript levels. PCR conditions included an initial denaturation at 95°C followed by 40–50 cycles of denaturation at 95°C for 15 sec and annealing/extension at 60°C for 30 sec. Primer sequences used for U2-type and U12-type introns are provided in Supplementary Table 1. Splicing efficiency was calculated as a ratio of relative quantities of spliced and unspliced pre-mRNA levels and was set as 1 for the control transduced cells.

Overexpression of ZRSR2

Full length coding sequence of human *ZRSR2* gene (1449 bp) was amplified using PCR and cloned into BamHI/NotI sites of pCDNA3.1 expression vector (Invitrogen). 2 μg plasmid was used to transfect 293T cells in a 60 mm petri dish using jetPRIME transfection reagent (Polyplus Transfection) according to the manufacturer's protocol. RNA was extracted 72 hours after transfection and overexpression of *ZRSR2* was verified using qPCR. RTPCR to assess the splicing efficiency of U12-type introns was performed as described above.

Bone marrow samples

Bone marrow aspirates of diagnostic samples including MDS and non-malignant cases were obtained at the MLL Munich Leukemia Laboratory. Informed consent was obtained in accordance with the Declaration of Helsinki and approved by the Institutional Review Board of the MLL. Unfractionated bone marrow mononuclear cells were lyzed, and total RNA was extracted using RNeasy Kit (Qiagen).

Soft-agar colony assay

Colony forming ability of TF-1 and K562 cells was determined by plating the cells in semi-solid media containing agar. The bottom layer consisted of 0.5% agar supplemented with 20% FBS, RPMI-1640 medium and antibiotics/antimycotic (Gibco). 1500 cells were mixed with the top agar layer which contained 0.35% agar and RPMI-1640 medium, FBS, L-Glutamine, β-mercaptoethanol and antibiotics/antimycotic, which was plated in each well of 24-well dish. 2 weeks after plating, colonies were enumerated under the microscope from triplicate wells.

Xenograft tumor model

All mice experiments were approved by the Institutional Animal Care and Use Committee, National University of Singapore, Singapore. Ten million K562 cells were resuspended in 50% matrigel and injected subcutaneously into flank of eight weeks old female NOD-scid-gamma (NSG) mice. Each mouse was injected with control cells in one flank and the ZRSR2 knockdown cells in the other. Once tumors were palpable, mice were sacrificed, tumors were harvested and weighed.

In vitro differentiation of human CD34+ cells

CD34+ cells were enriched from fresh cord blood and transduced twice, 24 hours apart, with ZRSR2 shRNA lentivirus. For colony assay, 2,500 transduced cells were plated per well in a 6-well dish in methylcellulose media (Stemcell Technologies) supplemented with SCF, G-

CSF, GM-CSF, IL-3 and EPO and containing puromycin. Colonies were enumerated after 9 days. In some experiments, cells were harvested from colonies and used to extract RNA. Downregulation of *ZRSR2* was examined using qRT-PCR. For liquid culture, cells were maintained in the presence of SCF, GM-CSF, IL-3, EPO and puromycin for 2 weeks. Expression of Glycophorin A and CD71 (erythroid lineage) and CD11b (myeloid lineage) was determined using flow cytometry. Data were analyzed using Flowjo software.

RNA sequencing

Library preparation, sequencing and mapping—cDNA libraries were prepared using TruSeq RNA Sample Preparation Kit (Illumina) according to the manufacturer's protocol. 1 μg of total RNA was used for library preparation and paired end adapters were ligated to DNA fragments prior to amplification and sequencing on a HiSeq 2000 instrument (Illumina) with 100 bp paired end reads according to manufacturer's protocol. We first mapped the sequenced reads to the reference transcript in the database obtained from RefSeq, Ensemble and UCSC known genes using bowtie and unmapped or poorly mapped reads were realigned to human reference genome (hg19) with the Blat software. This two-step mapping procedure is included in genomon-fusion (http://genomon.hgc.jp/rna/) pipeline.

The mapped reads were organized into five different libraries a) exon read library, 2) intron read library, 3) exon-intron junction read library, 4) exon-exon junction read library, and 5) intergenic read library. The gene classification was done using all known RefSeq transcripts. In order to be considered as a real junction, two criteria were applied. Firstly, we required the splice junction to be supported by at least 5 reads, and aligned reads spanned a minimal of 4 bp on each side of the junction.

Differential splicing analysis—In order to identify splicing events, we introduced a parameter called Mis-splicing Index (MSI), which is equivalent to Percent Spliced in (PSI) values used for alternative splicing analysis[67,68] and modified to cater to different splicing events such as intron retention, exon skip, and incorrect splice site usage (see Supplementary Fig. 5 for mathematical expression of MSI). For identification of differential splicing between two samples, the difference in MSI (MSI) was applied: MSI = $MSI_{ZRSR2\ mutant}$ – $MSI_{control}$. Furthermore, we used the Fisher's exact test to evaluate the significance of such difference and adjusted p value by FDR analysis to minimize the false positives. For identification of differentially spliced events among two genotypes, we performed all possible pairwise analyses between *ZRSR2* mutant MDS and control (*ZRSR2* WT MDS and normal BM) samples. These include 32 comparisons each between '*ZRSR2* mutant MDS' and '*ZRSR2* WT MDS' or '*ZRSR2* mutant MDS' and 'normal BM' (total 64 pairwise comparisons). As control, *ZRSR2* WT MDS samples were compared to normal BM samples ($4 \times 4 = 16$ comparisons). Similar approach was used to compare the rate of mis-splicing in ZRSR2 knockdown vs control transduced TF-1 cells. Statistical difference of p 0.01 and difference in Mis-splicing Index (MSI) of >20 were considered as significant differential splicing in each comparison. To identify an overall significant mis-splicing between the two genotypes (*ZRSR2* mutant vs controls), we considered the frequency of occurrence of mis-splicing events in pairwise comparisons and applied a FDR of 0.01 for intron retention and

0.02 for abnormal splice site recognition and exon skip analysis, using the control-vs-control comparisons as background.

For intron retention analysis, we selected events where at least 1 read overlaps an intron and flanking exons at each of the two junctions and the total number of such junction read counts was a minimum of 4, in at least one sample. We also applied the criteria that 95% of the intron was covered by at least 1 read (Supplementary Fig. 17).

Classification of introns—First, position weight matrices were generated based on the 5' and 3' splice sites and the branch site sequence. These matrices were used to scan the introns of interest, and the introns were then categorized as U2-type or U12-type based on the mapping score[27].

Gene expression analysis—The relative abundance of transcripts was quantified using normalized fragments per kilobase of transcript per million fragments mapped (FPKM), which were calculated using bedtools with a transcriptome reference.

Gene function analysis for mis-spliced genes—Genes significantly mis-spliced in *ZRSR2* mutant MDS cases were analyzed using Gene Ontology (GO) tools to identify enriched GO terms for biological pathways, biological processes and molecular functions. Significant enrichment was computed based on the Fishers' exact test using the numbers of mis-spliced genes compared to the numbers in the genome for each GO term. The obtained P value was further corrected for false discovery rate as described[69]. GO pathway analysis tool used was the MetaCore from GeneGO (https://portal.genego.com/) and the GO analysis for biological processes and molecular functions was done with DAVID (http://david.abcc.ncifcrf.gov). The corrected P value cutoff of 0.05 was used for significant enriched GO terms. Heat maps were created for enriched biological processes and molecular functions using Cluster 3.0 software.

Validation of mis-spliced genes—Intron retention in *ZRSR2* mutant MDS was verified using qRT-PCR[70]. Expression of each intron was normalized against the expression of flanking exons. For validation of other mis-spliced introns, qPCR or conventional PCR were used. *GAPDH* was used as the normalization control for cDNA input. Primer sequences are available in the Supplementary Table 1.

Supplementary Material

Refer to Web version on PubMed Central for supplementary material.

ACKNOWLEDGEMENTS

REFERENCES

1. Hofmann WK, Koeffler HP. Myelodysplastic syndrome. Annu Rev Med. 2005; 56:1–16. [PubMed: 15660498]

2. Greenberg PL. The multifaceted nature of myelodysplastic syndromes: clinical, molecular, and biological prognostic features. J Natl Compr Canc Netw. 2013; 11:877–884. quiz 885. [PubMed: 23847221]

3. Ma X. Epidemiology of myelodysplastic syndromes. Am J Med. 2012; 125:S2–S5. [PubMed: 22735748]

4. Tefferi A, Vardiman JW. Myelodysplastic syndromes. N Engl J Med. 2009; 361:1872–1885. [PubMed: 19890130]

5. Sekeres MA, Bejanyan N. The revolution of myelodysplastic syndromes. Ther Adv Hematol. 2011; 2:33–43. [PubMed: 23556074]

6. Shih AH, Abdel-Wahab O, Patel JP, Levine RL. The role of mutations in epigenetic regulators in myeloid malignancies. Nat Rev Cancer. 2012; 12:599–612. [PubMed: 22898539]

7. Schlegelberger B, Gohring G, Thol F, Heuser M. Update on cytogenetic and molecular changes in myelodysplastic syndromes. Leuk Lymphoma. 2012; 53:525–536. [PubMed: 21877899]

8. Yoshida K, et al. Frequent pathway mutations of splicing machinery in myelodysplasia. Nature. 2011; 478:64–69. [PubMed: 21909114]

9. Maciejewski JP, Padgett RA. Defects in spliceosomal machinery: a new pathway of leukaemogenesis. Br J Haematol. 2012; 158:165–173. [PubMed: 22594801]

10. Thol F, et al. Frequency and prognostic impact of mutations in SRSF2, U2AF1, and ZRSR2 in patients with myelodysplastic syndromes. Blood. 2012; 119:3578–3584. [PubMed: 22389253]

11. Makishima H, et al. Mutations in the spliceosome machinery, a novel and ubiquitous pathway in leukemogenesis. Blood. 2012; 119:3203–3210. [PubMed: 22323480]

12. Graubert TA, et al. Recurrent mutations in the U2AF1 splicing factor in myelodysplastic syndromes. Nat Genet. 2012; 44:53–57. [PubMed: 22158538]

13. Damm F, et al. Mutations affecting mRNA splicing define distinct clinical phenotypes and correlate with patient outcome in myelodysplastic syndromes. Blood. 2012; 119:3211–3218. [PubMed: 22343920]

14. Papaemmanuil E, et al. Clinical and biological implications of driver mutations in myelodysplastic syndromes. Blood. 2013

15. Lamond AI. The spliceosome. Bioessays. 1993; 15:595–603. [PubMed: 8240312]

16. Hall SL, Padgett RA. Conserved sequences in a class of rare eukaryotic nuclear introns with non-consensus splice sites. J Mol Biol. 1994; 239:357–365. [PubMed: 8201617]

17. Tarn WY, Yario TA, Steitz JA. U12 snRNA in vertebrates: evolutionary conservation of 5' sequences implicated in splicing of pre-mRNAs containing a minor class of introns. RNA. 1995; 1:644–656. [PubMed: 7489523]

18. Tarn WY, Steitz JA. A novel spliceosome containing U11, U12, and U5 snRNPs excises a minor class (AT-AC) intron in vitro. Cell. 1996; 84:801–811. [PubMed: 8625417]

19. Tarn WY, Steitz JA. Highly diverged U4 and U6 small nuclear RNAs required for splicing rare AT-AC introns. Science. 1996; 273:1824–1832. [PubMed: 8791582]

20. Will CL, Luhrmann R. Splicing of a rare class of introns by the U12-dependent spliceosome. Biol Chem. 2005; 386:713–724. [PubMed: 16201866]

21. Patel AA, Steitz JA. Splicing double: insights from the second spliceosome. Nat Rev Mol Cell Biol. 2003; 4:960–970. [PubMed: 14685174]

22. Tronchere H, Wang J, Fu XD. A protein related to splicing factor U2AF35 that interacts with U2AF65 and SR proteins in splicing of pre-mRNA. Nature. 1997; 388:397–400. [PubMed: 9237760]

23. Shen H, Zheng X, Luecke S, Green MR. The U2AF35-related protein Urp contacts the 3' splice site to promote U12-type intron splicing and the second step of U2-type intron splicing. Genes Dev. 2010; 24:2389–2394. [PubMed: 21041408]

24. Hall SL, Padgett RA. Requirement of U12 snRNA for in vivo splicing of a minor class of eukaryotic nuclear pre-mRNA introns. Science. 1996; 271:1716–1718. [PubMed: 8596930]

25. Fu Y, Masuda A, Ito M, Shinmi J, Ohno K. AG-dependent 3'-splice sites are predisposed to aberrant splicing due to a mutation at the first nucleotide of an exon. Nucleic Acids Res. 2011; 39:4396–4404. [PubMed: 21288883]

26. Kitamura T, et al. Establishment and characterization of a unique human cell line that proliferates dependently on GM-CSF, IL-3, or erythropoietin. J Cell Physiol. 1989; 140:323–334. [PubMed: 2663885]

27. Sheth N, et al. Comprehensive splice-site analysis using comparative genomics. Nucleic Acids Res. 2006; 34:3955–3967. [PubMed: 16914448]

28. Alioto TS. U12DB: a database of orthologous U12-type spliceosomal introns. Nucleic Acids Res. 2007; 35:D110–D115. [PubMed: 17082203]

29. Chen HZ, Tsai SY, Leone G. Emerging roles of E2Fs in cancer: an exit from cell cycle control. Nat Rev Cancer. 2009; 9:785–797. [PubMed: 19851314]

30. Gery S, Gombart AF, Fung YK, Koeffler HP. C/EBPepsilon interacts with retinoblastoma and E2F1 during granulopoiesis. Blood. 2004; 103:828–835. [PubMed: 12947005]

31. Kikuchi J, et al. E2F-6 suppresses growth-associated apoptosis of human hematopoietic progenitor cells by counteracting proapoptotic activity of E2F-1. Stem Cells. 2007; 25:2439–2447. [PubMed: 17600109]

32. Trikha P, et al. E2f1-3 are critical for myeloid development. J Biol Chem. 2011; 286:4783–4795. [PubMed: 21115501]

33. Kadri Z, et al. Direct binding of pRb/E2F-2 to GATA-1 regulates maturation and terminal cell division during erythropoiesis. PLoS Biol. 2009; 7:e1000123. [PubMed: 19513100]

34. Zhang J, et al. pRB and E2F4 play distinct cell-intrinsic roles in fetal erythropoiesis. Cell Cycle. 2010; 9:371–376. [PubMed: 20023434]

35. Kinross KM, Clark AJ, Iazzolino RM, Humbert PO. E2f4 regulates fetal erythropoiesis through the promotion of cellular proliferation. Blood. 2006; 108:886–895. [PubMed: 16861343]

36. Chan G, Gu S, Neel BG. Erk1 and Erk2 are required for maintenance of hematopoietic stem cells and adult hematopoiesis. Blood. 2013; 121:3594–3598. [PubMed: 23444405]

37. Chung E, Hsu CL, Kondo M. Constitutive MAP kinase activation in hematopoietic stem cells induces a myeloproliferative disorder. PLoS One. 2011; 6:e28350. [PubMed: 22164275]

38. Chung E, Kondo M. Role of Ras/Raf/MEK/ERK signaling in physiological hematopoiesis and leukemia development. Immunol Res. 2011; 49:248–268. [PubMed: 21170740]

39. Hsu CL, Kikuchi K, Kondo M. Activation of mitogen-activated protein kinase kinase (MEK)/ extracellular signal regulated kinase (ERK) signaling pathway is involved in myeloid lineage commitment. Blood. 2007; 110:1420–1428. [PubMed: 17536016]

40. Geest CR, Coffer PJ. MAPK signaling pathways in the regulation of hematopoiesis. J Leukoc Biol. 2009; 86:237–250. [PubMed: 19498045]

41. Stone JC. Regulation and Function of the RasGRP Family of Ras Activators in Blood Cells. Genes Cancer. 2011; 2:320–334. [PubMed: 21779502]

42. Kamata T, et al. A critical function for B-Raf at multiple stages of myelopoiesis. Blood. 2005; 106:833–840. [PubMed: 15784729]

43. Machnicki MM, Stoklosa T. BRAF--a new player in hematological neoplasms. Blood Cells Mol Dis. 2014; 53:77–83. [PubMed: 24495477]

44. Nelson DS, et al. Somatic activating ARAF mutations in Langerhans cell histiocytosis. Blood. 2014; 123:3152–3155. [PubMed: 24652991]

45. Zhang J, et al. PTEN maintains haematopoietic stem cells and acts in lineage choice and leukaemia prevention. Nature. 2006; 441:518–522. [PubMed: 16633340]

46. Yilmaz OH, et al. Pten dependence distinguishes haematopoietic stem cells from leukaemia-initiating cells. Nature. 2006; 441:475–482. [PubMed: 16598206]

47. Visconte V, et al. SF3B1 haploinsufficiency leads to formation of ring sideroblasts in myelodysplastic syndromes. Blood. 2012; 120:3173–3186. [PubMed: 22826563]

48. Przychodzen B, et al. Patterns of missplicing due to somatic U2AF1 mutations in myeloid neoplasms. Blood. 2013; 122:999–1006. [PubMed: 23775717]

49. Damm F, et al. SF3B1 mutations in myelodysplastic syndromes: clinical associations and prognostic implications. Leukemia. 2012; 26:1137–1140. [PubMed: 22064355]

50. Malcovati L, et al. Clinical significance of SF3B1 mutations in myelodysplastic syndromes and myelodysplastic/myeloproliferative neoplasms. Blood. 2011; 118:6239–6246. [PubMed: 21998214]

51. Wu SJ, et al. The clinical implication of SRSF2 mutation in patients with myelodysplastic syndrome and its stability during disease evolution. Blood. 2012; 120:3106–3111. [PubMed: 22932795]

52. Meggendorfer M, et al. SRSF2 mutations in 275 cases with chronic myelomonocytic leukemia (CMML). Blood. 2012; 120:3080–3088. [PubMed: 22919025]

53. Will CL, et al. The human 18S U11/U12 snRNP contains a set of novel proteins not found in the U2-dependent spliceosome. RNA. 2004; 10:929–941. [PubMed: 15146077]

54. Turunen JJ, Will CL, Grote M, Luhrmann R, Frilander MJ. The U11-48K protein contacts the 5' splice site of U12-type introns and the U11-59K protein. Mol Cell Biol. 2008; 28:3548–3560. [PubMed: 18347052]

55. Argente J, et al. Defective minor spliceosome mRNA processing results in isolated familial growth hormone deficiency. EMBO Mol Med. 2014; 6:299–306. [PubMed: 24480542]

56. Jackson IJ. A reappraisal of non-consensus mRNA splice sites. Nucleic Acids Res. 1991; 19:3795–3798. [PubMed: 1713664]

57. Turunen JJ, Niemela EH, Verma B, Frilander MJ. The significant other: splicing by the minor spliceosome. Wiley Interdiscip Rev RNA. 2013; 4:61–76. [PubMed: 23074130]

58. Edery P, et al. Association of TALS developmental disorder with defect in minor splicing component U4atac snRNA. Science. 2011; 332:240–243. [PubMed: 21474761]

59. He H, et al. Mutations in U4atac snRNA, a component of the minor spliceosome, in the developmental disorder MOPD I. Science. 2011; 332:238–240. [PubMed: 21474760]

60. Otake LR, Scamborova P, Hashimoto C, Steitz JA. The divergent U12-type spliceosome is required for pre-mRNA splicing and is essential for development in Drosophila. Mol Cell. 2002; 9:439–446. [PubMed: 11864616]

61. Konig H, Matter N, Bader R, Thiele W, Muller F. Splicing segregation: the minor spliceosome acts outside the nucleus and controls cell proliferation. Cell. 2007; 131:718–729. [PubMed: 18022366]

62. Markmiller S, et al. Minor class splicing shapes the zebrafish transcriptome during development. Proc Natl Acad Sci U S A. 2014; 111:3062–3067. [PubMed: 24516132]

63. Boultwood J, Dolatshad H, Varanasi SS, Yip BH, Pellagatti A. The role of splicing factor mutations in the pathogenesis of the myelodysplastic syndromes. Adv Biol Regul. 2013

64. Moran-Crusio K, et al. Tet2 loss leads to increased hematopoietic stem cell self-renewal and myeloid transformation. Cancer Cell. 2011; 20:11–24. [PubMed: 21723200]

65. Li Z, et al. Deletion of Tet2 in mice leads to dysregulated hematopoietic stem cells and subsequent development of myeloid malignancies. Blood. 2011; 118:4509–4518. [PubMed: 21803851]

66. Haferlach T, et al. Landscape of genetic lesions in 944 patients with myelodysplastic syndromes. Leukemia. 2014; 28:241–247. [PubMed: 24220272]

67. Wang ET, et al. Alternative isoform regulation in human tissue transcriptomes. Nature. 2008; 456:470–476. [PubMed: 18978772]

68. Shapiro IM, et al. An EMT-driven alternative splicing program occurs in human breast cancer and modulates cellular phenotype. PLoS Genet. 2011; 7:e1002218. [PubMed: 21876675]
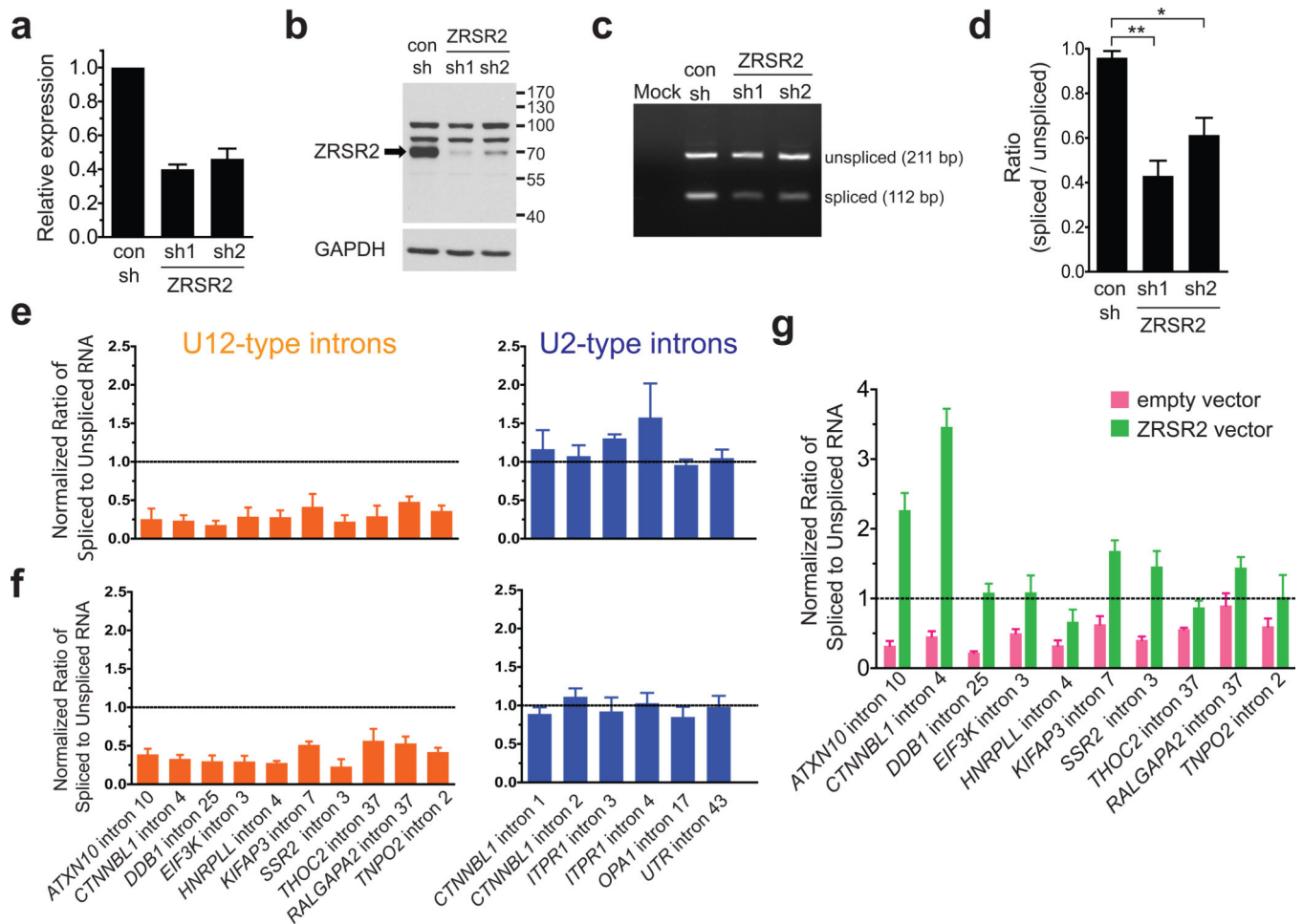
69. Benjamini Y, Hochberg Y. Controlling the false discovery rate: a practical and powerful approach to multiple testing. J.R. Statist. Soc. B. 1995; 57:289–300.

70. Wong JJ, et al. Orchestrated intron retention regulates normal granulocyte differentiation. Cell. 2013; 154:583–595. [PubMed: 23911323]

Figure 1. Knockdown of ZRSR2 induces defects in splicing of U12-type introns

(**a**) Transcript levels of *ZRSR2* in TF-1 cells stably transduced with either lentiviral ZRSR2 shRNA or control (con) vectors were examined using quantitative RT-PCR. *GAPDH* levels served as endogenous control. (**b**) Western blot analysis to verify the decrease in ZRSR2 protein levels in knockdown TF-1 cells. (**c**) Splicing efficiency of Intron F of *P120* minigene construct was measured in ZRSR2 knockdown and control 293T cells. A representative gel picture shows bands corresponding to unspliced and spliced product in RT-PCR analysis performed 48h after transfection of minigene plasmid. (**d**) The bars depict ratio of intensities of PCR bands corresponding to spliced and unspliced products in *P120* minigene assay. The data represent the mean ± SEM of three independent transfection experiments. *P < 0.05, **P <0.01; Unpaired t test. (**e** and **f**) Average ratio of spliced to unspliced pre-mRNA levels of ten U12-type and six U2-type introns in TF-1 cells upon knockdown of ZRSR2 using two shRNA vectors, ZRSR2 sh1 (**e**) and ZRSR2 sh2 (**f**). The data are mean ± SEM from at least 3 independent RNA preparations. Horizontal dotted lines represent the ratio for control transduced cells which were set as 1.0. *GAPDH* was used as endogenous control. (**g**) Average ratios of spliced to unspliced levels of U12-type introns upon transient transfection of ZRSR2 expression plasmid in knockdown 293T cells are depicted. 293T cells stably expressing ZRSR2 sh1 or control vector were transfected with either pCDNA3-hZRSR2 or

empty vector and total RNA was extracted after 72h. The splicing efficiency was measured using qPCR and spliced/unspliced ratio was set as 1.0 for control cells transfected with empty vector (horizontal dotted line). *GAPDH* was used to normalize for cDNA input. The results are average of 5–7 transfection experiments and represented as mean ± SEM.
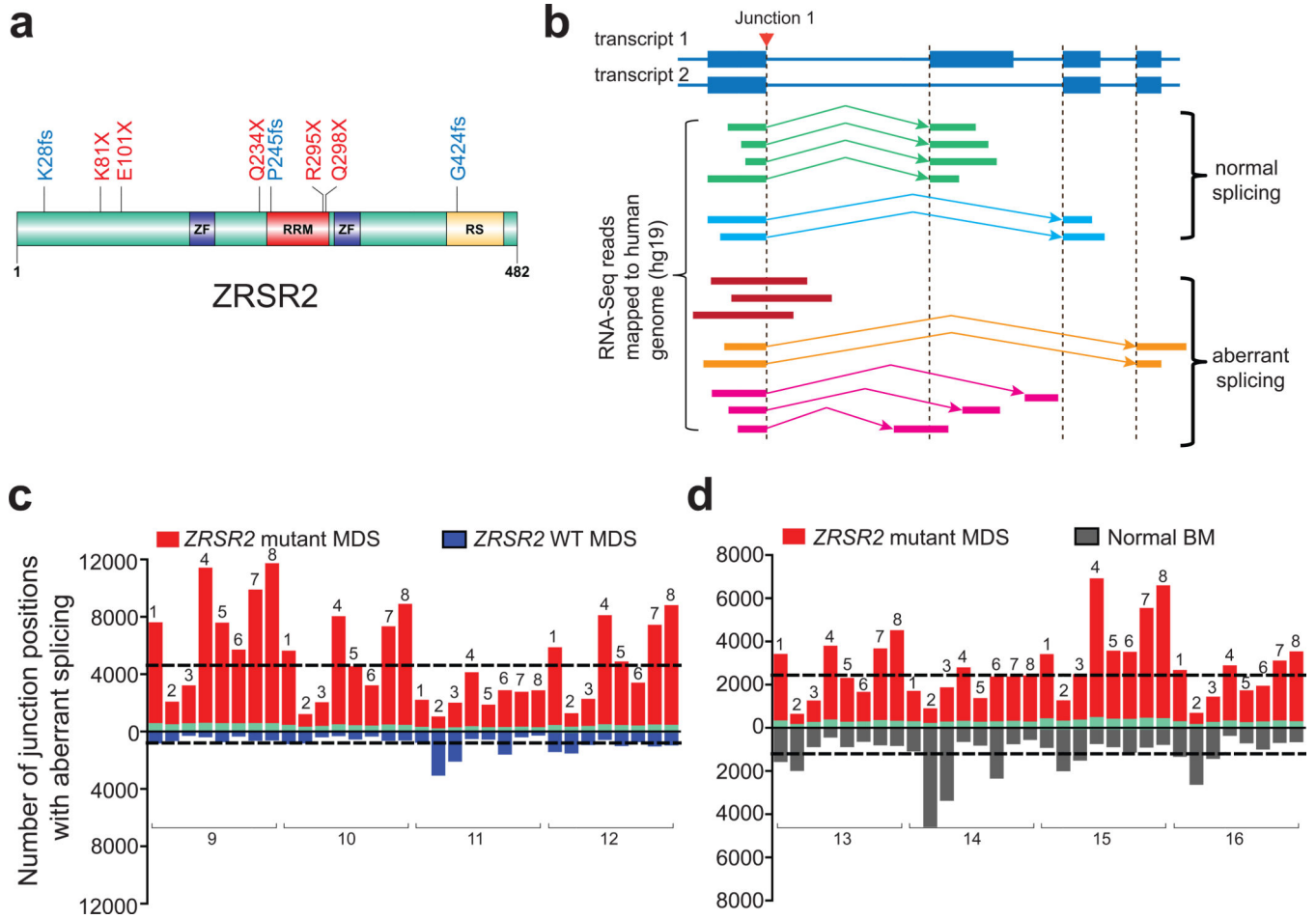
Figure 2. RNA sequencing of MDS bone marrow harboring mutations in *ZRSR2* reveals splicing defects

(**a**) Schematic representation of human ZRSR2 protein with position and type of mutations in eight MDS patients used for RNA-Seq. (**b**) Approach used to define the RNA-Seq reads for analysis of splice junctions is shown. All splice junctions corresponding to known RefSeq transcripts were examined. Reads mapped to a representative splice position (Junction 1) are classified as either 'normal' or 'aberrant' in the illustration. (**c**) Number of junction positions with aberrant reads obtained in pairwise comparisons between *ZRSR2* mutant and WT MDS are depicted. Junctions with significant aberrant reads in *ZRSR2* mutant (MSI>20) are shown as red bars while those in *ZRSR2* WT (MSI<-20) are shown as blue bars for each mutant vs WT pair. The dashed horizontal lines denote the averages of aberrant junction positions in the two genotypes across 32 comparison pairs (eight *ZRSR2* mutant MDS compared individually to four *ZRSR2* WT MDS). (**d**) Number of aberrant junctions obtained in pairwise comparisons between *ZRSR2* mutant MDS and normal BM analyzed and depicted as described in (c). The black bars represent number of aberrant junctions detected in normal BM. The green bars in (c) and (d) represent the number of junctions which were identified in all eight mutant / eight control samples in at least one pairwise comparison. Each pair of bars in (c) and (d) is labelled with identifiers for *ZRSR2*

mutant and control samples represented in their pair-wise comparison. The sample information including details of ZRSR2 mutations are described in Table 1.
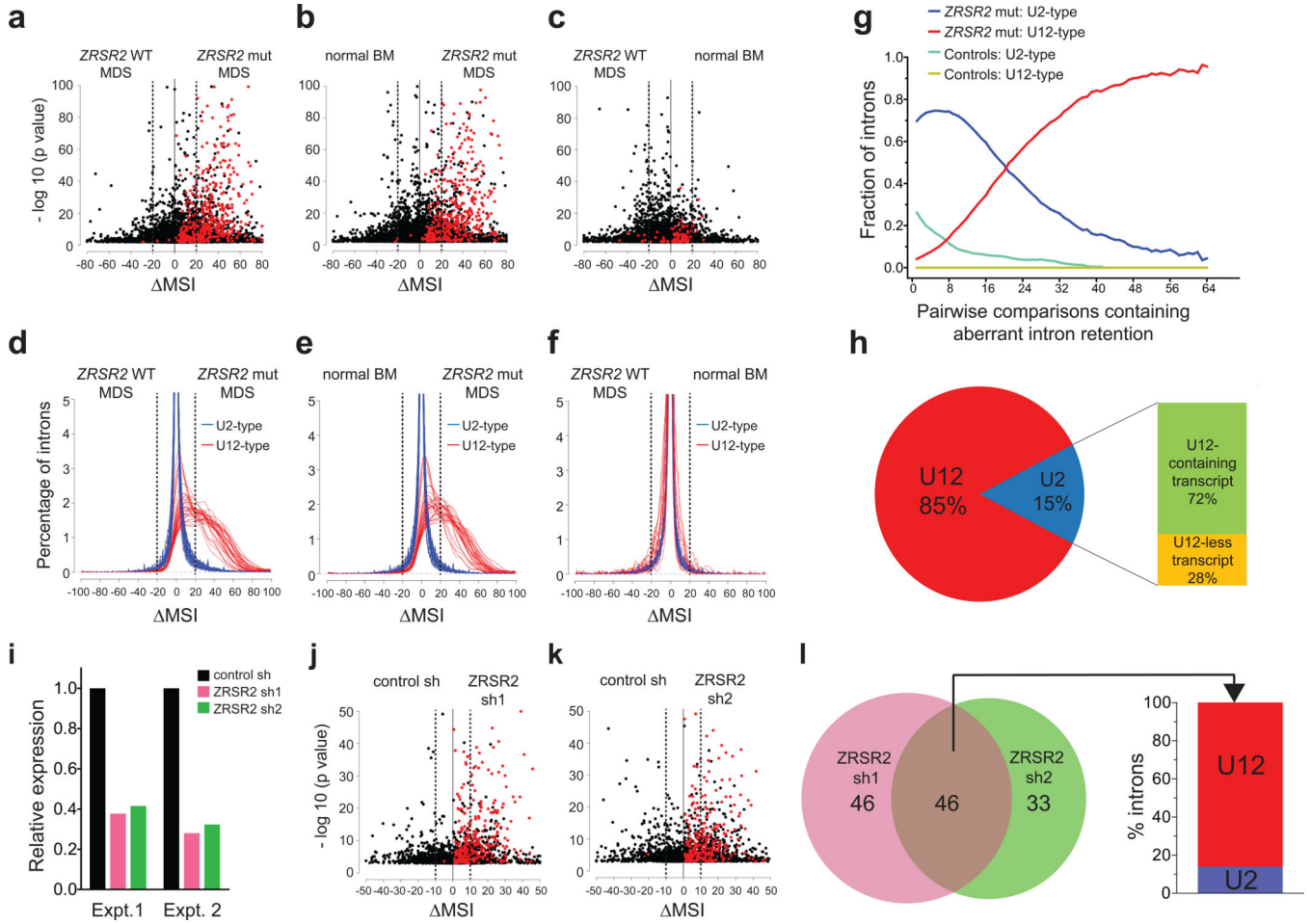
Figure 3. *ZRSR2* mutated MDS bone marrow and ZRSR2 knockdown cells are characterized by aberrant retention of U12-type introns

(**a–c**) Dot plots display aberrantly retained introns in a representative pairwise analysis of *ZRSR2* mutant MDS vs *ZRSR2* WT MDS (a), *ZRSR2* mutant MDS vs normal BM (b) and normal BM vs *ZRSR2* WT MDS (c). Each dot denotes an intron and U12-type introns are shown in red. p value was calculated using Fisher's exact test and data points with p<0.01 are shown. (**d–f**) Histograms depict frequencies of U2-type and U12-type introns plotted against MSI value in pairwise comparisons of *ZRSR2* mutant and control samples. Each curve represents a pairwise comparison for U2-type (blue) and U12-type (red) intron. 32 comparisons between *ZRSR2* mutant MDS and *ZRSR2* WT MDS (d), 32 comparisons between *ZRSR2* mutant MDS and normal BM (e), and 16 comparisons between *ZRSR2* WT MDS and normal BM (**f**) were performed. (**g**) The proportion of U2-type and U12-type introns among aberrantly retained introns in either *ZRSR2* mutant or controls (*ZRSR2* WT MDS + normal BM) are shown for 64 pairwise comparisons. The number of introns is plotted against the number of pairwise comparisons in which they were identified. (**h**) Distribution of intron type for significantly retained introns (MSI>20; FDR 0.01) in *ZRSR2* mutant MDS is shown. The bar graph shows the distribution of retained U2-type introns into those present in either transcript containing a U12-type intron or without U12-type intron. (**i**) Relative expression of *ZRSR2* was computed as FPKM values from RNA-

Seq data in two independently transduced control and knockdown TF-1 cells. (**j–k**) Dot plots depict aberrantly retained introns in control vs ZRSR2 sh1 (j) and control vs ZRSR2 sh2 (k). Only data points corresponding to p<0.01 are displayed. (**l**) Venn diagram shows an overlap of retained introns between ZRSR2 sh1 and sh2 knockdown TF-1 cells. The introns which are significantly retained (p<0.01;   MSI>10) for sh1 or sh2 transduced cells in both experiments are included. The bar graph on the right depicts the proportion of U2-type and U12-type introns among the introns retained in both sh1 and sh2 transduced cells.
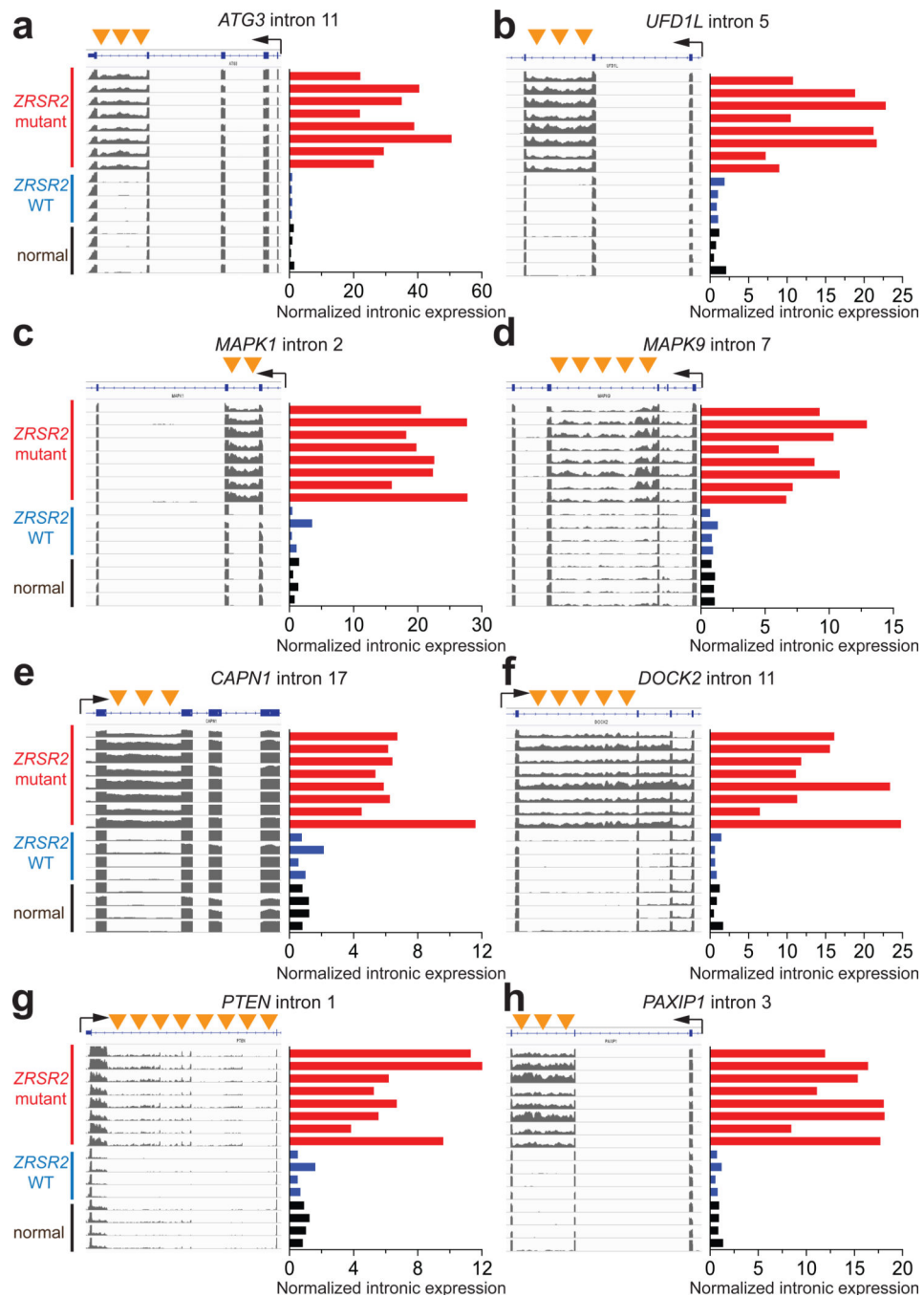
Figure 4. Detection of U12-type intron retention in *ZRSR2* mutant MDS

(**a–h**) Normalized intron expression for eight representative U12-type introns was determined using quantitative PCR. The RNA-Seq reads normalized to total number of mappable reads for all 16 cases are depicted using IGV 2.3 in the left panels. Read counts are shown using an identical scale in all samples, and the U12-type introns are indicated by orange arrow heads. For each gene, only the genomic locus containing the retained intron is shown. Right panels: The expression of U12-type introns was measured relative to the

expression of flanking exons and is shown by horizontal bars (red bars: *ZRSR2* mutant MDS; blue bars: *ZRSR2* WT MDS; black bars: normal BM).

Author Manuscript

Author Manuscript

Author Manuscript

Author Manuscript
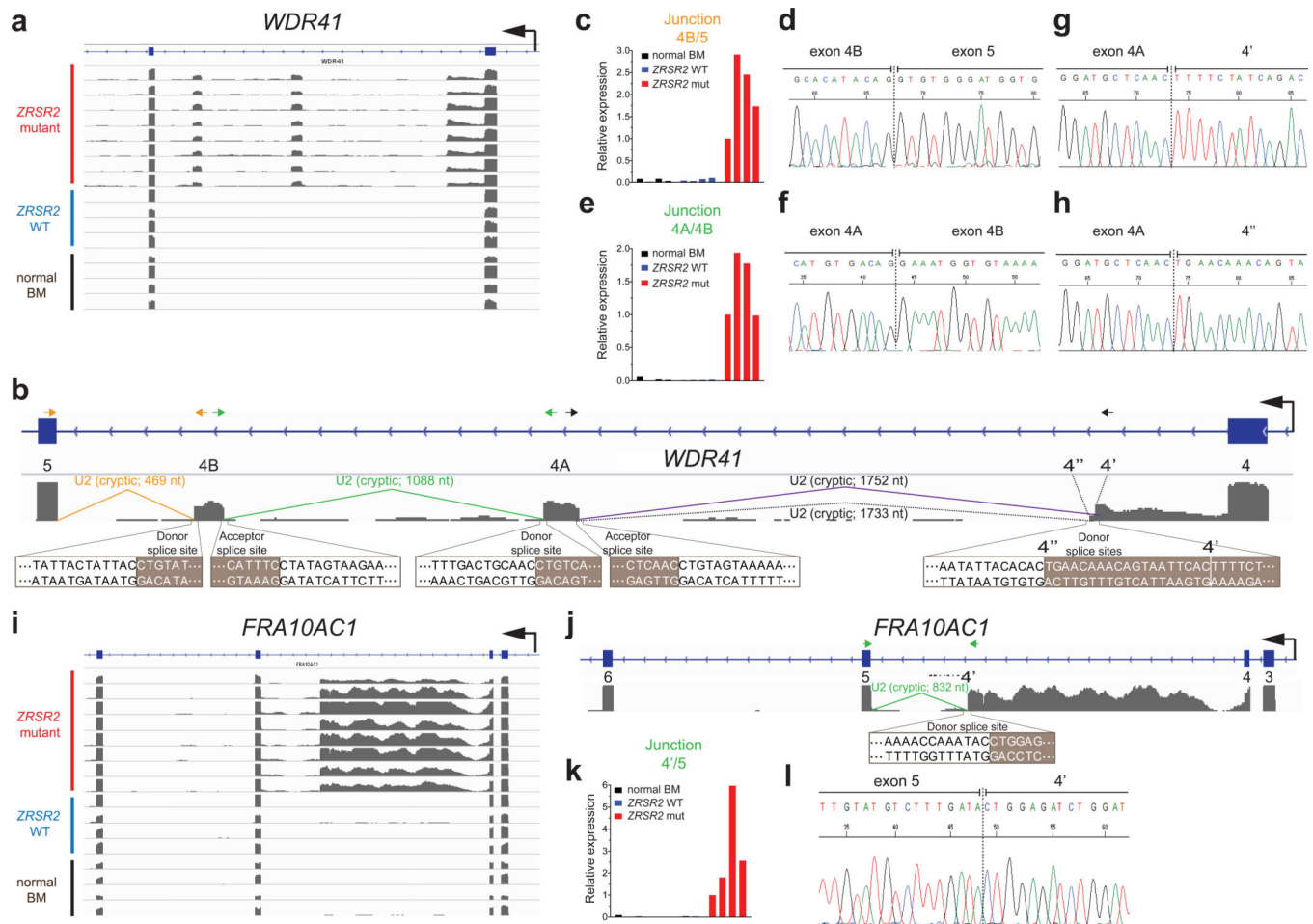
Figure 5. Cryptic splice junctions in U12-type introns of *WDR41* and *FRA10AC1*
(**a**) Normalized RNA-Seq reads mapped to the genomic region encompassing exons 4 and 5 of *WDR41* gene are displayed using IGV 2.3 for all 16 samples. Reads in all samples are shown on identical scale. (**b**) Aberrant splice junctions in intron 4 (U12-type intron) of *WDR41* gene are depicted. The mis-spliced regions (designated 4A and 4B) and two alternative splice donor sites in intron 4 (upstream of 4A; marked as 4' and 4") in *ZRSR2* mutant samples are illustrated. The intron type and length for the cryptic junctions are indicated. The cryptic splice acceptor and donor sequences which are activated in *ZRSR2* mutant MDS are shown below. The PCR primers used in (c) and (e) are indicated by arrows. (**c–d**) Experimental verification of splicing junction between 4B and exon 5 of *WDR41*. (**c**) qRT-PCR using primers located in 4B and exon 5 to determine relative levels of mis-spliced transcript in *ZRSR2* mutant and control samples. (**d**) The PCR product amplified from cDNA of *ZRSR2* mutant samples in (c) was Sanger sequenced. The junction is shown by dashed vertical line. (**e–f**) Splicing between 4A and 4B was analyzed as described above in (c) and (d), respectively. (**g–h**) Sanger sequencing of the PCR amplicon obtained from cDNA of *ZRSR2* mutant samples using primers located in 4A and retained intron (upstream of 4'). The PCR product was cloned into TOPO TA vector and individual clones were sequenced to verify two alternative splice donor sites (4' and 4"). (**i**) RNA-Seq reads mapped to the genomic region encompassing exons 3–6 of *FRA10AC1* gene. (**j**) Aberrant

splice donor site (denoted 4') in intron 4 of *FRA10AC1* is shown for a representative *ZRSR2* mutant sample. Sequence and intron-type for the cryptic splice junction are indicated. (**k**) qRT-PCR to measure the relative levels of mis-spliced RNA in *ZRSR2* mutant and control samples using primers located in intron 4 and exon 5. *GAPDH* was used to normalize the levels of transcripts. (**l**) Sanger sequencing of the PCR product obtained from *ZRSR2* mutant samples in (j). The junction between intron 4 and exon 5 is indicated by the dashed vertical line.
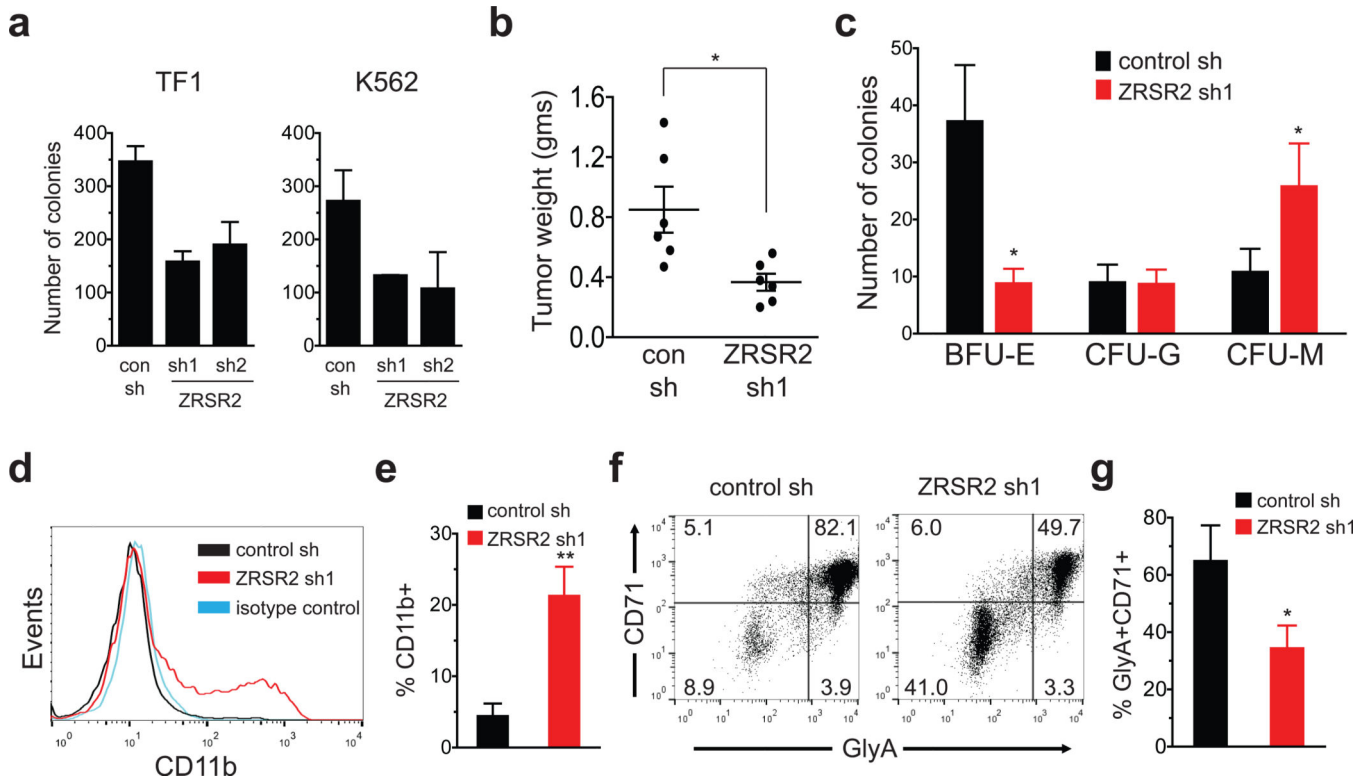
Figure 6. Stable knockdown of ZRSR2 alters cell growth and differentiation
(**a**) Colony forming ability of TF-1 and K562 cells transduced with ZRSR2 shRNA and control vectors was evaluated using soft-agar colony assay. 1500 cells were seeded in each well of a 24-well plate, and colonies were enumerated after 2 weeks. Cells were plated in triplicate, and the data are the mean ± SEM from multiple experiments (TF-1: n=8 for sh1 and n=3 for sh2; K562: n=2) (**b**) ZRSR2 knockdown and control K562 cells were transplanted into the flank of NSG mice; tumors were dissected after 2 weeks and weighed. Data represent mean ± SEM. (**c**) Cord blood derived CD34$^+$ cells were transduced with ZRSR2 shRNA lentivirus and plated in methylcellulose media containing SCF, IL3, GCSF, GMCSF and EPO as well as 1 µg/ml puromycin. BFU-E, CFU-G and CFU-M colonies were counted after 9 days. Data represent the mean ± SEM of three experiments. (**d–g**) CD34+ cells were transduced as in (c), cultured in liquid media containing SCF, IL3, GMCSF and EPO for 2 weeks and analyzed using flow cytometry. (**d**) A representative overlay of histograms showing staining with CD11b antibody used as a marker of differentiation towards myeloid lineage. (**e**) Percentage of CD11b$^+$ cells obtained after *in vitro* differentiation of CD34+ cells in 4 experiments are depicted (mean ± SEM). (**f**) Erythroid differentiation was measured using surface expression of Glycophorin A and CD71 antigens in cells cultured for 2 weeks in the presence of cytokines. Representative dot plots for FACS staining in ZRSR2 knockdown and control cells are shown. Percentage of cells in each quadrant are indicated. (**g**) Bar graphs represent percentages of GlyA$^+$CD71$^+$ cells from 3 experiments (mean ± SEM). *P<0.05, **P<0.01. P values were calculated using Student's t test.
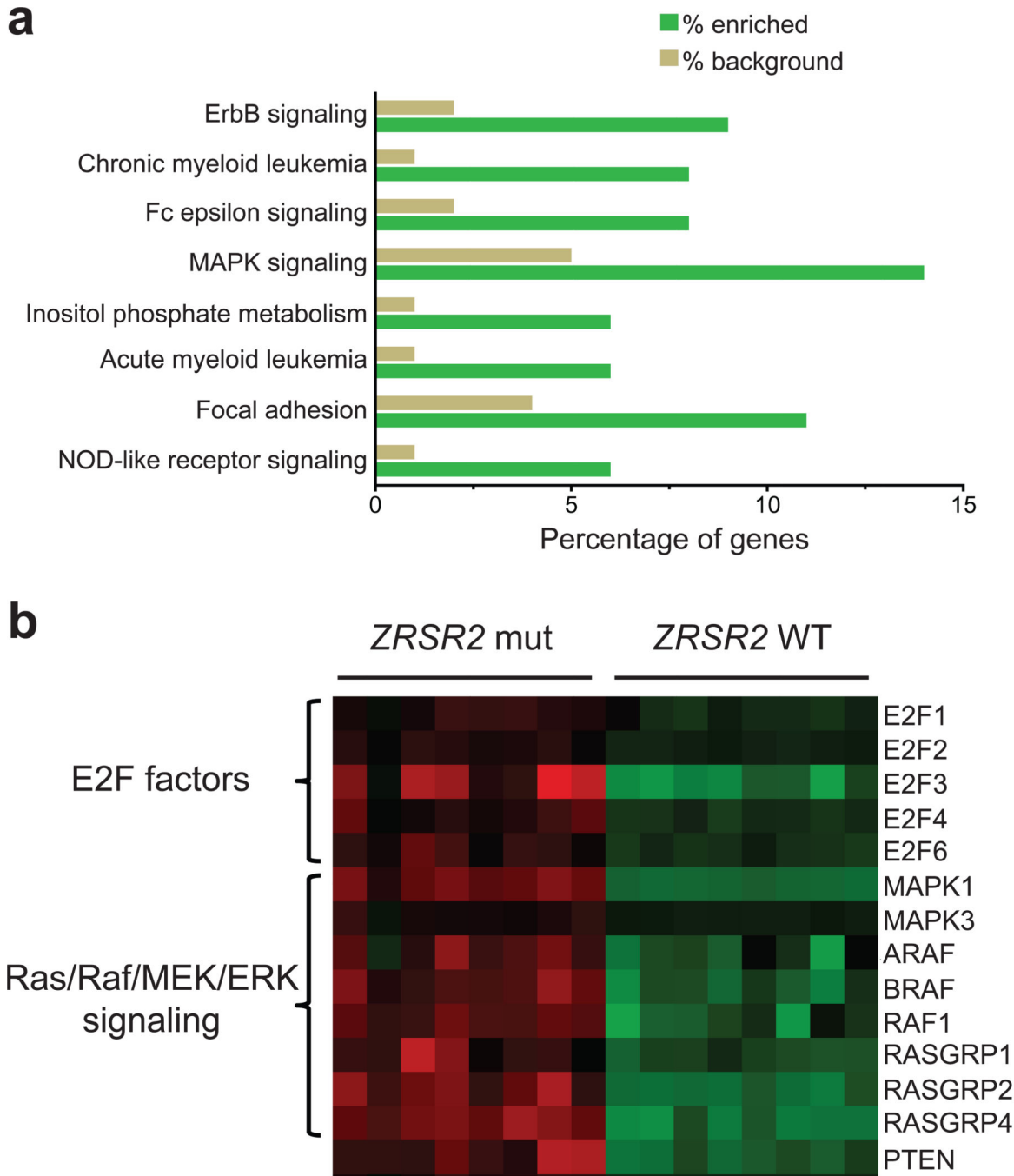
Figure 7. Gene Ontology (GO) analyses of mis-spliced genes in *ZRSR2* mutant MDS
(**a**) GO analysis of 251 significantly mis-spliced genes in *ZRSR2* mutant MDS shows their enrichment in a number of essential biological pathways (p<0.05). (**b**) Heat map portrays the relative scale of aberrant retention of U12-type introns in genes involved in hematopoietic development. MSI values for U12-type introns in *ZRSR2* mutant and control samples were utilized for depiction of mis-splicing.

Table 1

Details of human bone marrow samples used for RNA-Seq

Sample #	MDS / normal	Age	Gender	ZRSR2 mutation[a] Nucleotide	Protein	WHO subtype	IPSS[b]	Cytogenetics
1	MDS	59	Male	C892T	Gln298X	RAEB-1	1	46,XY
2	MDS	81	Male	G301T	Glu101X	RA	1	45,X,-Y
3	MDS	70	Male	A241T	Lys81X	RCMD	0	46,XY
4	MDS	74	Male	81delA	Lys28fsX11	RCMD	0	46,XY
5	MDS	72	Male	C883T	Arg295X	RCMD	0	46,XY
6	MDS	74	Male	C700T	Gln234X	RAEB-2	2	46,XY
7	MDS	62	Male	1271delG	Gly424fsX93	RAEB-2	2	46,XY
8	MDS	72	Male	735delC	Pro245fsX9	RCMD	0	46,XY
9	MDS	50	Male	-	-	RA	1	46,XY,t(2;11)(p21:q23)
10	MDS	76	Male	-	-	RAEB-2	3	45,XY,-7
11	MDS	65	Female	-	-	RAEB-1	1	46,XX
12	MDS	71	Male	-	-	RA	0	45,X,-Y
13	Remission state of #7	62	Male	-	-	-	-	NA[c]
14	normal BM	51	Male	-	-	-	-	46,XY
15	normal BM	38	Male	-	-	-	-	46,XY
16	normal BM	75	Male	-	-	-	-	46,XY

[a]None of the MDS samples harbor mutation in other frequently mutated spliceosome genes: *SF3B1*, *SRSF2* and *U2AF1*

[b]International Prognostic Scoring System IPSS (0=low; 1=int-1; 2=int-2; 3=high)

[c]Not available